Charging of insulators by multiply-charged-ion impact probed by slowing down of fast binary-encounter electrons

E. De Filippo,[1] G. Lanzanó,[1,*] F. Amorini,[2] G. Cardella,[1] E. Geraci,[1,3] L. Grassi,[1,3] E. La Guidara,[1,4] I. Lombardo,[2,3] G. Politi,[1,3] F. Rizzo,[2,3] P. Russotto,[2,4] C. Volant,[5] S. Hagmann,[6,7] and H. Rothard[8,†]

[1]*Istituto Nazionale di Fisica Nucleare Sezione di Catania, Via S. Sofia 64, I-95123 Catania, Italy*

[2]*Istituto Nazionale di Fisica Nucleare-Laboratori Nazionali del Sud, LNS, Via S. Sofia 62, I-95123 Catania, Italy*

[3]*Dipartimento di Fisica e Astronomia, Via S. Sofia 64, I-95123 Catania, Italy*

[4]*Centro Siciliano Fisica Nucleare e Struttura della Materia, CSFNSM, Catania, Italy*

[5]*Département Astrophysique, physique des Particules, physique Nucléaire et de l'Instrumentation Associée/Service de Physique Nucléaire, CEA/Saclay, F-91191 Gif-sur-Yvette, France*

[6]*GSI Helmholtzzentrum für Schwerionenforschung, D-64291 Darmstadt, Germany*

[7]*Institut für Kernphysik IKF, J. W. Goethe Universität, Frankfurt am Main, Germany*

[8]*Centre de Recherche sur les Ions, les Matériaux et la Photonique, CIMAP-CIRIL-Ganil (CEA/CNRS/ENSICAEN/Université de Caen-Basse Normandie), BP 5133, F-14070 Caen Cedex 05, France*

(Received 8 September 2010; published 7 December 2010)

The interaction of ion beams with insulators leads to charging-up phenomena, which at present are under investigation in connection with guiding phenomena in nanocapillaries with possible application in nanofocused beams. We studied the charging dynamics of insulating foil targets [Mylar, polypropylene (PP)] irradiated with swift ion beams (C, O, Ag, and Xe at 40, 23, 40, and 30 MeV/u, respectively) via the measurement of the slowing down of fast binary-encounter electrons. Also, sandwich targets (Mylar covered with a thin Au layer on both surfaces) and Mylar with Au on only one surface were used. Fast-electron spectra were measured by the time-of-flight method at the superconducting cyclotron of Laboratori Nazionali del Sud (LNS) Catania. The charge buildup leads to target-material-dependent potentials of the order of 6.0 kV for Mylar and 2.8 kV for PP. The sandwich targets, surprisingly, show the same behavior as the insulating targets, whereas a single Au layer on the electron and ion exit side strongly suppresses the charging phenomenon. The accumulated number of projectiles needed for charging up is inversely proportional to electronic energy loss. Thus, the charging up is directly related to emission of secondary electrons.

DOI: 10.1103/PhysRevA.82.062901 PACS number(s): 34.35.+a, 34.50.Fa, 79.20.−m

I. INTRODUCTION

The interaction of ionizing radiation with insulators may induce a buildup of charge on the target surface. Both the injected charge of the primary particle and the emission of secondary electrons contribute [1–4]. This phenomenon has been studied extensively for electron-beam impact [2–4], and it is of particular importance for electron microscopy [4]. With multiply charged heavy ions, much bigger secondary electron yields occur as compared to that seen with electron or proton impact. Therefore, charging phenomena should be more important in the former case. Charging-up affects methods for materials analysis based on charged-particle beams or the analysis of charged ejected "secondary" particles. In many cases it may become difficult to apply methods such as ion scattering, secondary electron- and secondary ion spectroscopy, Auger Electron Spectroscopy (AES), Secondary Ion Mass Spectrometry (SIMS), and even x-ray emission Particle Induced x-ray Emission (PIXE) to the analysis of insulators [5].

Charging-up under multiply charged ion irradiation is at present under investigation in connection with guiding phenomena in nanocapillaries, with possible application in nanofocused beams [6,7]. The experimental studies have triggered some interesting numerical investigations [8], and first applications with high-energy beams emerge [9]. Most experimental investigations rely on measurements of transmitted beam angular distributions and charge states. Conclusions about quantitative aspects of charging can only be drawn by means of sophisticated multi-time-scale numerical simulations: As pointed out by Schiessl *et al.* [8], a specificity of charging-up phenomena following ion impact and ionization is that enormously wide-ranging time scales are simultaneously present. The primary ionization takes places in the sub-fs range and electronic relaxation in conductors occurs within 1 to 10 fs. The charge buildup itself, depending on the projectile and the beam current, occurs on a scale ranging from less than a femtosecond up to several hours. There is a lack of clear-cut measurements of even basic quantities such as the induced built-up potential and its corresponding electric field.

For more than 10 years, the ARGOS multidetector, initially designed for the detection and identification of nuclear reaction products and their energies in a wide angular range [10], has been used with great success in the domain of atomic collision physics, since it allows also the study of the emission of fast electrons [11–14]. The studies focused on binary-encounter electrons [11,14], convoy electrons [13,15], fast electrons produced by the "Fermi shuttle" mechanism [12,13], and also Auger electrons from the in-flight deexcitation of electron-carrying projectiles [15]. After a pilot experiment at Grand Accelerateur National d'Ions Lourds (Caen) [16], dedicated experiments on charging-up phenomena were conducted at the

*Deceased.
†rothard@ganil.fr

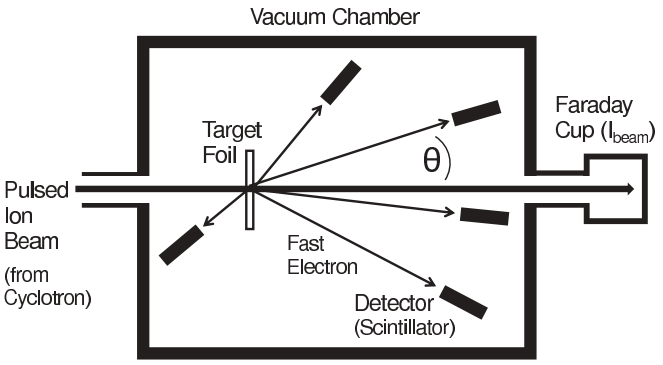

FIG. 1. Experimental setup (schematic, see text).

CS (Superconductor Cyclotron) of Istituto Nazionale di Fisica Nucleare-LNS (Catania) with insulating foils. The charging dynamics was measured via the slowing down of fast electrons: Their velocity was obtained by the time-of-flight method using the scintillation detectors of the multidetector ARGOS.

Here we report on the dependence of the charging up of Mylar and polypropylene (PP) on the amount of energy deposited in the target by the fast projectiles. The measurement of the irradiation-time-dependent slowing down of fast binary-encounter electrons (BEEs) makes it possible to measure the charging-up-induced BEE energy shift, and the projectile-dependent charging-up time constant in a direct and clear-cut way.

II. EXPERIMENT

Beams of C^{4+} (40 MeV/u), O^{4+} (23 MeV/u), O^{5+} (23 MeV/u), Ag^{30+} (40 MeV/u), and Xe^{31+} (30 MeV/u) delivered by the superconducting cyclotron CS were used to irradiate thin foils in the large scattering chamber CICLOPE or in the CHIMERA chamber of LNS. Figure 1 shows a sketch of the experimental setup. The beam traverses the target foils and the beam current I_{beam} is measured in a Faraday cup. When possible, the beam current was varied over orders of magnitude, in the range of about 2 pA $\leqslant I_{\text{beam}} \leqslant$ 350 pA, depending on the beam. The beam diameter ϕ on the target is 2 mm $\leqslant \phi \leqslant$ 3 mm.

In addition to conducting targets (Au of $\approx$100 μg/cm^2 thickness and several C foils in the range between $\approx$10 μg/cm^2 and $\approx$100 μg/cm^2), insulating PP of 4 μm thickness and Mylar ($\approx$100 μg/cm^2) foils were studied. Mylar (My) is the trade name of thin foils of polyethylene terephthalate (PET). Also, Au-My-Au sandwich targets (My of $\approx$100 μg/cm^2 thickness, covered with a thin Au layer of $\approx$10 μg/cm^2 on both surfaces), as well as Au-My foils (My covered with a thin Au layer of $\approx$10 μg/cm^2 on one surface), were used. The gold-coated surface was directed in the forward direction, that is, on the exit side of the ion beam and of the BEE. The targets were mounted as a "sandwich" between two thin metal frames, which assured electrical contact of the thin Au layers with the target holder. Up to 12 of these target frames were mounted on a target holder, which was either connected to a current digitizer to measure the target current I_{T} (with conducting targets), or simply grounded. The measurement of I_{T} and I_{beam} allows calculating the secondary electron emission yield γ [17,18].

The fast electrons were detected by means of fast scintillators coupled to photomultiplier tubes, as described in detail in [19]. In the large scattering chamber CICLOPE, 26 detectors were placed at a distance of 400 cm in a horizontal plane passing through the center of the target, at observation angles between $\theta = 1^\circ$ and $\theta = 24^\circ$. Another 10 detectors covered the backward angles between $\theta = 30^\circ$ and $\theta = 155^\circ$. In the CHIMERA chamber, 12 detectors covered the range $1.8^\circ \leqslant \theta \leqslant 26^\circ$, with a target-detector distance of 350 cm at 1.8°, decreasing to 283 cm at 26°. All data shown in the following were obtained with detectors mounted close to observation angles of $\theta = 9.2^\circ$. The residual pressure was about 10^{-6} mbar or lower.

The pulsed beam of CS-LNS (with a pulse width of typically 1 ns) makes it possible to measure the time of flight (TOF) of the electrons [11,19]: The pulsed beam radiofrequency was used as a start and the photomultiplier signal as a stop. The absolute electron velocity (or energy) is obtained by a calibration procedure using x rays or prompt γ rays from nuclear reactions in the target as reference for the velocity of light. In Figs. 2, 4, and 6, data involving the uncalibrated TOF are shown, since these are the initial raw data as they appear online during the experiment. From these initial data, after careful calibration, quantities such as the electron velocity (Fig. 3), the BEE energy (Figs. 5 and 7), and the BEE energy difference (Figs. 8 and 9) are deduced. The amplitude of the signal of the scintillation detector is a measure of the deposited energy and is proportional to the electron energy. In the present work, this feature is only used to set a window on the BEE peak, as shown in Fig. 2. This procedure makes it possible to clearly separate BEE from background and other ionization mechanisms such as electron transfer to the continuum (convoy electrons).

Figure 2 shows a plot of the energy deposited in the scintillation detector mounted at an observation angle of $\theta = 9.2^\circ$ as a function of the electron TOF. The collision systems are oxygen (23 MeV/u) on a (conducting) carbon target (top) and on an insulating Mylar target (bottom). Figure 3 shows the corresponding electron velocity distributions. One observes two prominent structures. BEEs appear at about twice the projectile velocity [1,11,14]. They stem from a knock-on ionization of target electrons by the projectile nucleus or, in other words, a Rutherford scattering of a target electron in the projectile's Coulomb field. This process is shown schematically in the inset of Fig. 3. The initial peak width is given by the "Compton profile" of the bound target electrons. The observed peak is broadened due to transport effects, that is, elastic and inelastic scattering of the electrons on their way from the point of ionization to the target surface [14,17,18]. If the Compton profile and the transport broadening are small enough, the intrinsic resolution of the spectrometer determines the observed peak width. With the ARGOS multidetector absolute cross sections for BEE emission have been measured with great precision. This allowed a stringent test of ionization theory [1,14,20], and the binary-encounter ionization process is now well understood.

Convoy electrons (CEs) originate from (target) electron capture or (projectile) electron loss to low-lying projectile continuum states. They have kinetic energies close to zero in the projectile frame and thus travel with the same velocity as

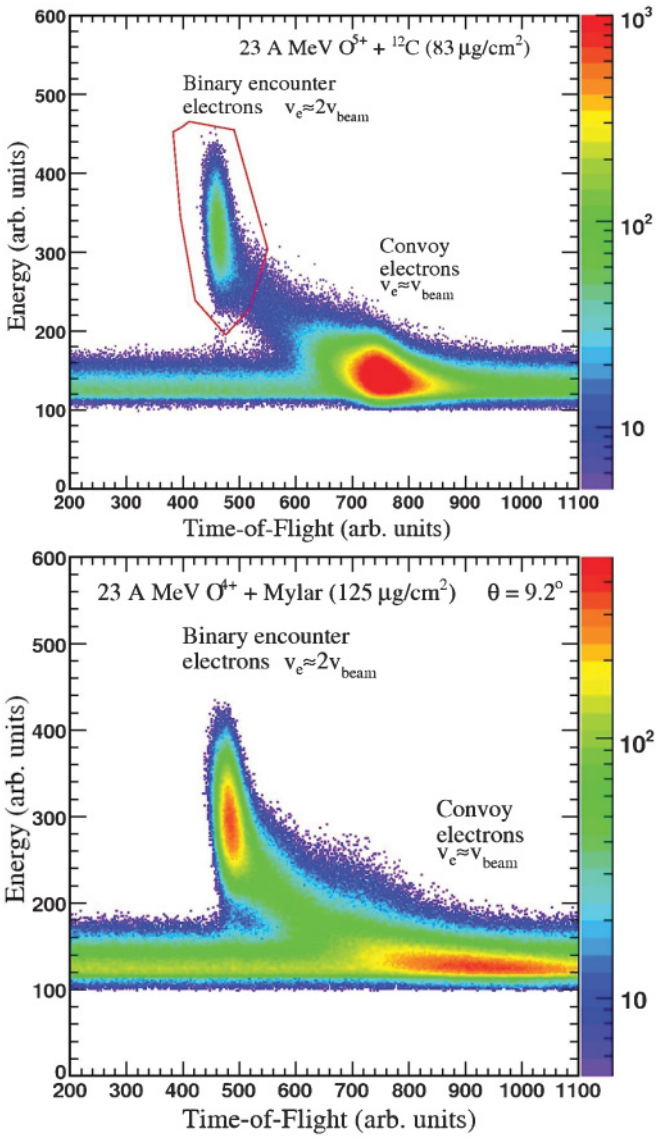

FIG. 2. (Color online) Energy deposited in the scintillator versus electron time-of-flight, for O beams (23 MeV/u) on carbon targets (top panel) and Mylar foils (bottom panel) for a detector mounted at an observation angle of $\theta = 9.2^\circ$.

the projectile. In the present experiment, amended scintillation detectors with a detection threshold of $E_{\mathrm{thr}} \approx 10$ keV were used, whereas in previous experiments [13], the threshold was $v_{\mathrm{thr}} \approx 7$ cm/ns, corresponding to almost $E_{\mathrm{thr}} \approx 20$ keV. After charging-up-induced slowing down, however, the energy of CEs falls below the detection threshold of the scintillation detectors in the case of projectiles with velocities below approximately 30 MeV/u [19]. This can be seen from the comparison of fast-electron ejection induced by 23 MeV/u oxygen ions from conducting carbon and insulating Mylar targets in Figs. 2 and 3. In the former case, both CEs and BEEs are clearly visible; in the latter case, only a pronounced BEE peak remains. Therefore, in the following we concentrate on the faster BEE as a probe of charging dynamics. Some observations concerning CE ejection from insulators and the influence of charging up were already discussed in Refs. [16,19,21–23].

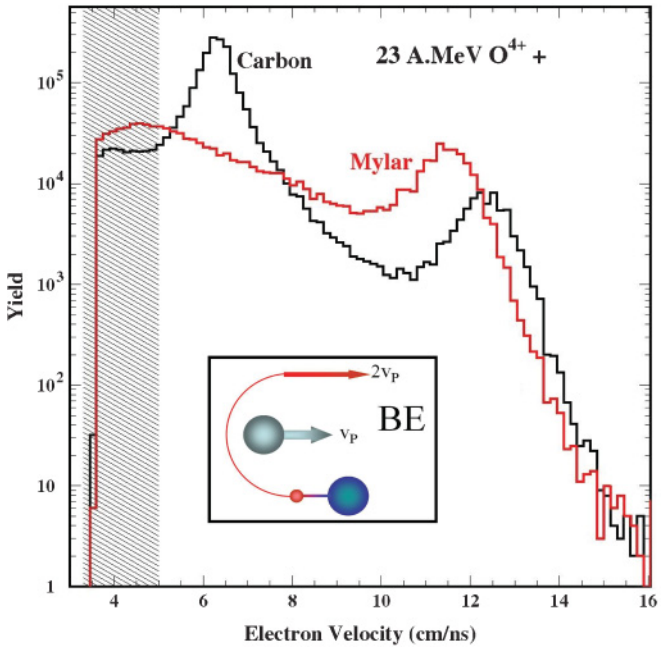

FIG. 3. (Color online) Forward electron velocity spectra from a C foil (conductor) and a Mylar target (insulator) irradiated by O beams (23 MeV/u). Observation angle $\theta = 9.2^\circ$. The inset shows a schematic drawing illustrating the "binary-encounter" ionization process (see text).

III. RESULTS: CHARGING UP DYNAMICS

As the insulator is irradiated, a charging up occurs either on the surface or in the bulk. The induced electrical field slows down the fast electrons. The ejection of low-energy "secondary" electrons (with energies below about 50 eV) is completely suppressed. As mentioned earlier, with conducting carbon targets, we were able to measure the beam-induced target current, which is mainly related to low-energy secondary electron emission [17,18]. No current could be measured with insulating targets indicating suppression of low-energy electron emission (the threshold for current measurement was $I_{\mathrm{T}} < 1$ pA). The charging up to potentials of several kV occurs typically on a time scale of some minutes. Already very low potentials of the order of 10–20 eV, which should be reached within a few seconds, are sufficient to inhibit emission of low-energy secondary electrons. At the very beginning of irradiation of insulators there should be a decrease of the induced target current, which could be measured with a dedicated experiment recording this time dependence of the induced target current, but that was outside the scope of the present experiment.

The charging effect on fast BEE emission can be seen in (Figs. 4–7). In (Figs. 4 and 6) the mean TOF of BEEs is shown as a function of irradiation time t. The evolution of the mean energy of BEEs is shown in (Figs. 5 and 7). As examples among the four different beams, the results for an oxygen beam ($Z_P = 8$; Figs. 4 and 5) and a heavy xenon ion beam ($Z_P = 54$, Figs. 6 and 7) were chosen. The same statistical method as reported in [16,19] is applied to the BEE peaks: (i) BEEs are separated from the background by choosing an appropriate window in the "deposited energy-TOF" bidimensional plot of

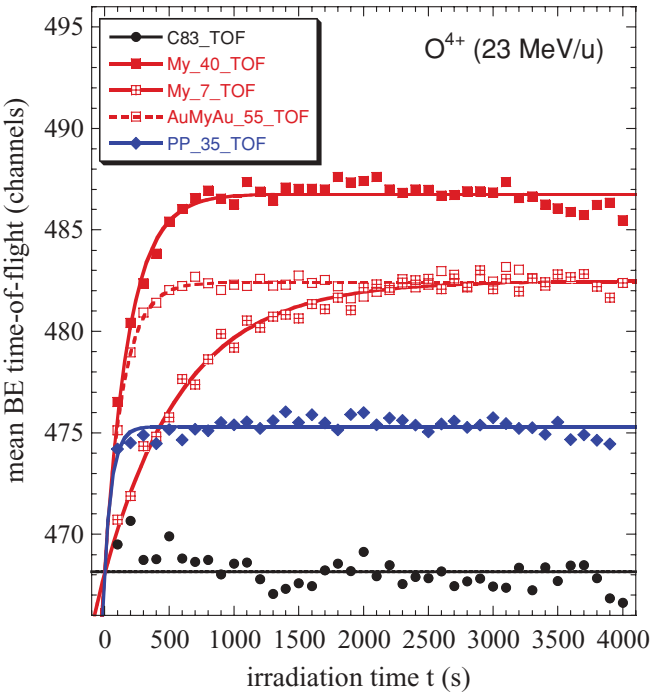

FIG. 4. (Color online) Mean time-of-flight (TOF) of BEEs induced by O^{4+} (23 MeV/u) as a function of irradiation time t for a Mylar target at two different ion beam currents of 7 pA (crossed open squares) and 40 pA (solid squares), an Au-Mylar-Au sandwich target at an ion beam current of 55 pA (open squares), a polypropylene (PP) target (diamonds) at an ion beam current of 35 pA, and a C foil of $\approx$83 μg/cm^2 (solid circles). The lines are fits of Eq. (1) to the data.

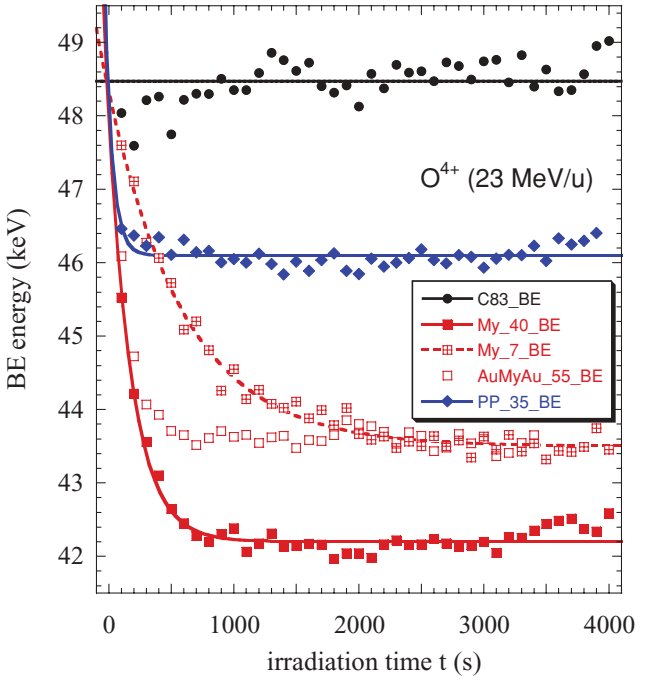

FIG. 5. (Color online) BEE energy (corresponding to the data of Fig. 4) as a function of irradiation time t for a Mylar target at two different ion beam currents of 7 pA (crossed open squares) and 40 pA (solid squares), an Au-Mylar-Au sandwich target (open squares), a polypropylene (PP) target (diamonds), and a C foil (solid circles, no shift; that is, the observed BEE energy of $\approx$48.5 keV remains constant).

Fig. 2. This cut, as shown in the top panel of Fig. 2, includes all the events from the beginning up to the end of the run. (ii) The elapsed time is stored together with all other information during the on-line acquisition. In the off-line analysis, the entire elapsed time during one run is divided in intervals Δt. The choice of the most appropriate Δt depends on the acquired statistics in this time interval and is of the order of 1 s $\leqslant \Delta t \leqslant$ 100 s, depending on the beam properties (projectile, current). (iii) Over each interval Δt, we calculate the average TOF by fitting a Gaussian distribution to the BEE peak and plot the BEE TOF as a function of irradiation time in Figs. 4 and 6. Figures 5 and 7 show the corresponding mean BEE energies as a function of irradiation time.

If a process of continuous, uniform charging-up of the insulator along the projectile trajectory or at the surface occurs, forward-emitted BEEs are slowed down, and TOF increases with elapsed irradiation time. This can clearly be observed with both Mylar and PP foils. The t dependence follows an exponential increase with a certain charging-up time constant τ: This behavior can well be described by a law of the form

$$\mathrm{TOF}(t) - T(\infty) = k[1 - \exp(t/\tau)], \qquad (1)$$

as shown in Figs. 4 and 6. This is modeling the time evolution of the dynamically trapped space charge as charging an equivalent RC circuit. In contrast, with a conducting C foil, the TOF remains constant. In the case of a conductor, electronic relaxation is very fast, the typical time scale is of the order of the plasmon frequency (0.1–1 fs), whereas in insulators, the relaxation time may be much longer.

The time constant τ depends on the ion-beam current: An example of the charging-up of Mylar with two different beam currents (7 and 40 pA) is shown in Figs. 4 and 5. The charging with the 40-pA beam is about 5 times faster than that with the 7-pA beam. However, within error bars, it is independent of the accumulated number of projectiles (fluence). Thus, a "dose effect" does not occur within detection limits; this can be seen from the two points obtained with the oxygen beam ($dE/dx \approx 1.5$ keV μg^{-1} cm^2) shown in Figs. 8 and 9. It should be emphasized that, for example, the difference between the asymptotic values for My at 40 pA and My at 7 pA corresponds to 0.4 ns, which is slightly below the resolution of the TOF measurements. Therefore, it is rather a measure of the error bars than an indication of a difference in TOF or final BEE energy.

Also, a dependence on the target material is observed. The charging-up of PP is faster than that of Mylar, but the absolute value of the resulting final electrical field is lower for PP than for Mylar. Another striking result here is that the charging dynamics observed with a Au-Mylar-Au sandwich target closely resembles that of the pure insulator Mylar. In contrast, a single Au layer on the electron- (and ion beam-) exit surface strongly reduces the peak shift and suppresses the slowing down (Figs. 6 and 7).

As one would naively expect, the single conducting Au layer seems to screen the outgoing electrons from the built-up electric field. The surprising result is that a double

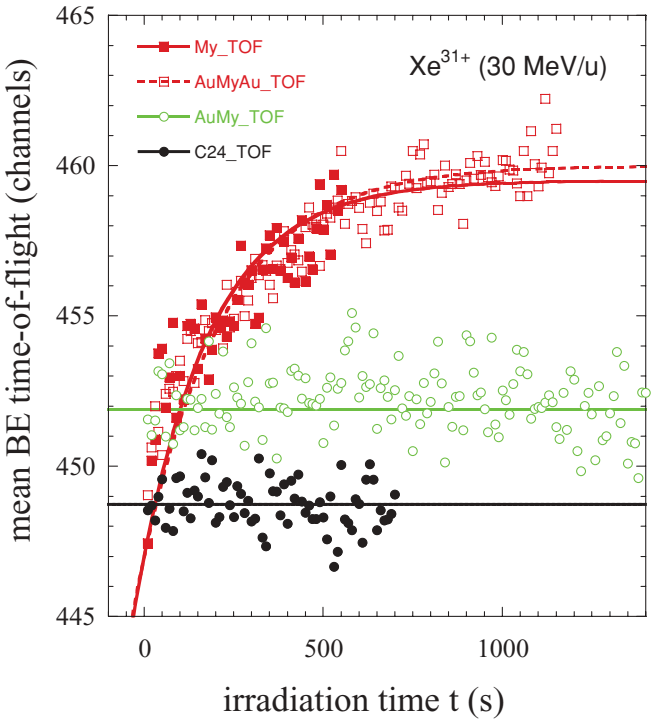

FIG. 6. (Color online) Mean time-of-flight (TOF) of BEE induced by Xe^{31+} (30 MeV/u, ion beam current 8 pA) as a function of irradiation time t for a Mylar target (solid squares, full curve), an Au-Mylar-Au sandwich target (open squares, dashed curve), a Mylar target covered with a single thin Au layer (open squares), and a C foil of ≈24 μg/cm^2 (solid circles).

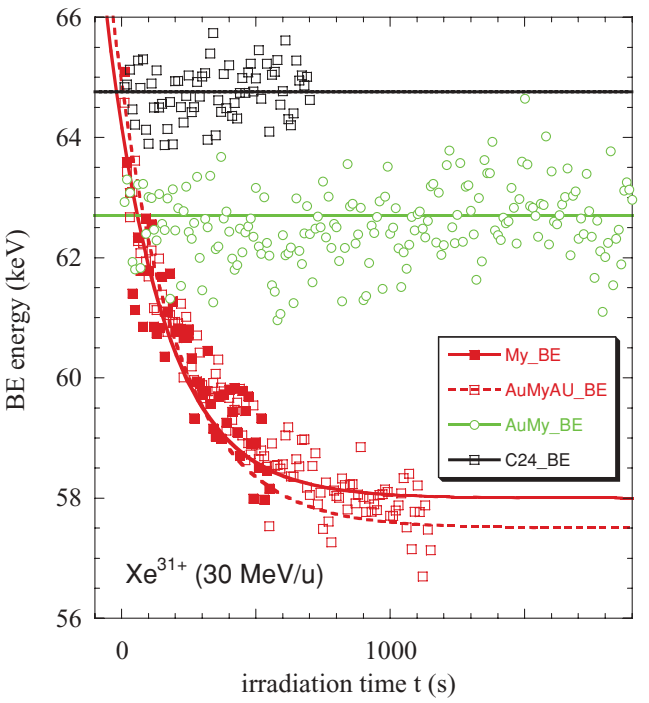

FIG. 7. (Color online) BEE energy (corresponding to the data of Fig. 6) of BEE induced by Xe^{31+} (30 MeV/u, ion beam current 8 pA) as a function of irradiation time t for a Mylar target (solid squares, full curve), an Au-Mylar-Au sandwich target (open squares, dashed curve), a Mylar target covered with a single thin Au layer (open squares), and a C foil (solid circles no shift; that is, the observed BEE energy of ≈65 keV remains constant).

layer behaves qualitatively as does the pure insulator. This may indicate that, in contrast to what was believed until now, a contribution from a bulk phenomenon, and not only macroscopic surface charging up, occurs. Indeed, Schiwietz *et al.* [23] observed slowing down of carbon *KLL* Auger electrons from PP foils bombarded with swift MeV/u heavy ions. Also, a shift of CE energy was observed with polymer foils [22]. Both observations are due to heavy-ion nuclear track potential, a "nanoscopic" effect related to a single-ion track, in contrast to a "macroscopic" surface charging as evoked in [16,21].

IV. INFLUENCE OF ELECTRONIC ENERGY LOSS AND TARGET MATERIAL

Swift heavy ions lose energy in matter mainly due to inelastic collisions with target electrons (electronic energy loss dE/dx) [1,24]. A basic question is how radiation effects (defect creation, particle emission, structural changes, etc.) evolve with the amount of deposited energy. Therefore, we performed experiments with several swift ions in a large range of dE/dx values. Two orders of magnitude were covered, from $dE/dx \approx 0.4$ keV μg^{-1} cm^2 to $dE/dx \approx 40$ keV μg^{-1} cm^2. The four dE/dx values of Figs. 8 and 9 belong to the four beams (C, O, Ag, Xe).

A simple observable for the charging dynamics is the number N of accumulated projectiles associated with the charging time constant τ of the exponential function of Eq. (1). This number N of accumulated projectiles needed to charge up the target completely is shown in Fig. 8(a) as a function of the energy loss dE/dx, which was calculated with the widely used SRIM software [24]. A simple power law is observed,

$$N \sim (dE/dx)^n, \tag{2}$$

with the exponent $n = -(0.94 \pm 0.08)$. Thus, in a good approximation, N is inversely proportional to dE/dx. Another possible scaling parameter would be the accumulated incoming projectile charge C_P needed to charge up the target, as shown in Fig. 8(b). Again, a simple proportionality $C_P \sim (dE/dx)^{-0.55}$ is observed. This can easily be understood from the fact that the energy loss is in a first approximation roughly proportional to the square of the projectile charge, $(dE/dx) \sim q^2$.

This finding shows that the charging up itself is directly related to ionization and the subsequent formation of a secondary electron cascade. The total number of the emitted secondary electrons was observed to be roughly proportional to the electronic energy loss dE/dx of the projectile. The total electron yield can be written as $\gamma = \Lambda\, dE/dx$ with the "material constant" Λ [1,17]. As said earlier, the measurement of I_T and I_{beam} allowed calculating γ, which was found to be $\gamma \approx 10$ ejected electrons per O^{q+} projectile at 23 MeV/u with a carbon target of ≈100 μg/cm^2 thickness. The ratio of γ and dE/dx, $\Lambda \approx 7$ keV^{-1} μg cm^{-2} is in good agreement with other data for C foils [1,17,18]. It is interesting to mention that a projectile charge state (O^{q+}) effect is observed with thinner targets of

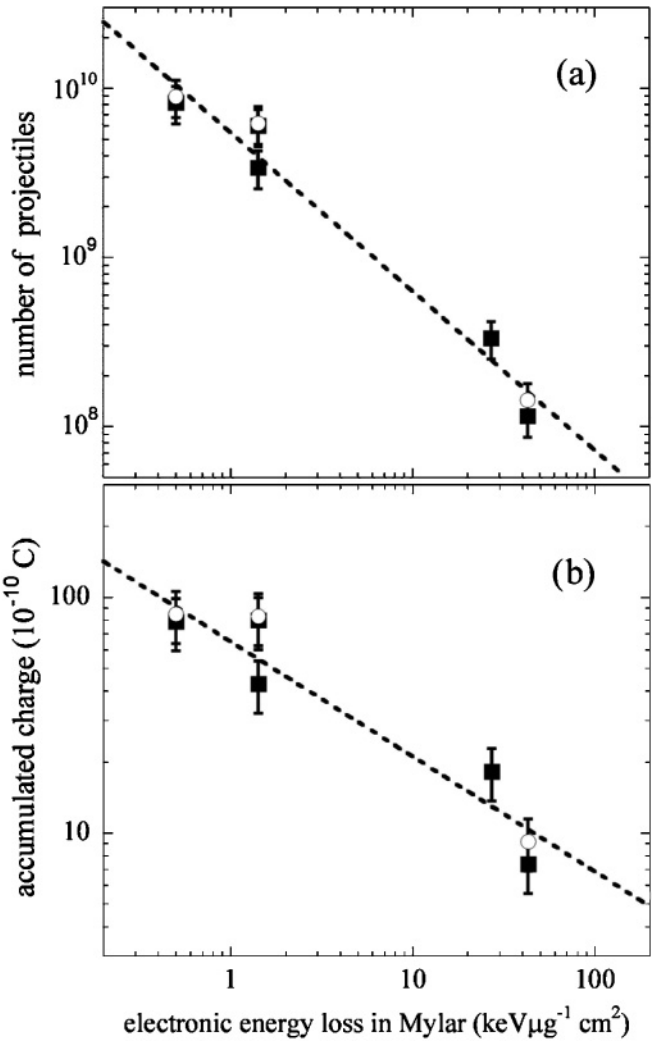

FIG. 8. Accumulated number N of projectiles (a) and accumulated charge (b) corresponding to the charging-up time constant τ of Eq. (1) as a function of electronic energy loss in the target (Mylar, solid squares; Au-Mylar-Au, open circles). The lines are fits of a power law $\sim(dE/dx)^n$ to the Mylar data (see text).

$\approx 10\,\mu$g/cm^2 thickness, $\gamma(q=5)\approx 7$ and $\gamma(q=4)\approx 6$, where the contributions of electron yields from both the entrance and the exit side of the foils to the total yield are nearly equal. In contrast, no charge effect is observed within error bars for thick targets where the forward-emitted electron yields become dominant and independent of target thickness, thus sweeping out the charge effect present on backward electron ejection [1,17,18].

The difference of the limit of the t-dependent BEE energy observed with insulators makes it possible, by subtracting them from the irradiation time-independent BEE energy obtained with conducting carbon foils, to calculate the charging-induced energy shift. This energy shift ΔE_{BEE} is equal to the induced slowing-down potential. This quantity is plotted as a function of the electronic energy loss in Fig. 9. The shift ΔE_{BEE} does not depend on dE/dx. On the other hand, a clear dependence on the target material is observed: For Mylar, the slowing-down potential amounts to $\approx$6.0 kV, and for PP it amounts to $\approx$2.8 kV. Bundaleski *et al.* also reported quite different

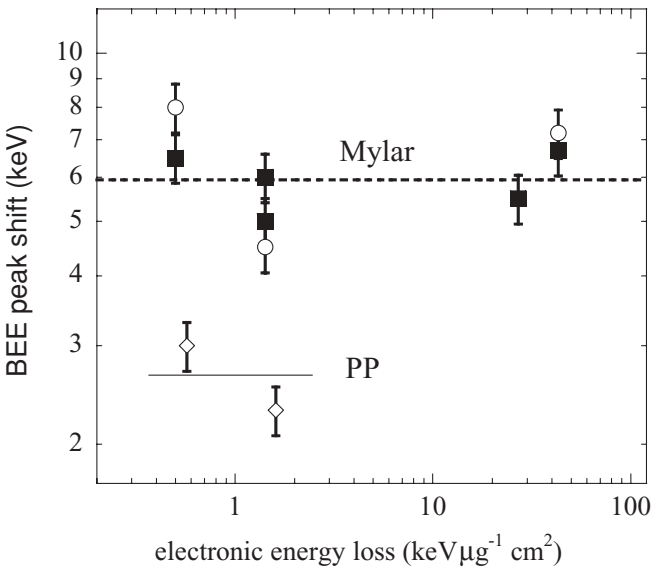

FIG. 9. Binary-encounter electron peak shift ΔE_{BEE} as a function of electronic energy loss in the target, for Mylar (solid squares), Au-My-Au sandwich targets (open circles), and polypropylene (open diamonds).

charging (and decharging) dynamics of various insulators irradiated with slow-ion beams, using an original method based on beam deflection under grazing incidence [25].

To model the charging behavior, one would need, besides the rather well-known ionization probability per unit path length per projectile, to know about the mobility of charge carriers in the polymers. In most polymers, conductivity is rather ionic than electronic [26]. When free electrons are generated, what is the gap to a possible conduction band in the two different insulators? How does the buildup of any possible electric field effect depend on these gaps and the trapping of thermalized electrons? Some efforts were made to calculate space-charge effects from such trapping of thermalized primary electrons in insulators [2,3] following electron-beam irradiation, also including PET (Mylar) [2]. For ionic projectiles, electrons do not come from the direct beam, but from primary ionization (including the binary-encounter process) and subsequent transport of electrons through the foils. These processes, however, should be close to processes occurring in carbon targets [14,18,20]. Unfortunately, it is not straightforward to search for a relation of the observed target material dependence with, for example, the electrical conductivity of the involved materials [26]. To give an idea, the electrical resistivity of Mylar is about 10^{20} Ωm. This is to be compared to that of a good conductor, such as gold (2.44×10^{-8} Ωm). The electrical properties of polymers do not only depend on their structure, but also on impurities and surface treatment [26].

V. CONCLUSION

The slowing down of fast BEEs allowed measuring the induced potential by ion irradiation of insulators in a simple, clear-cut way. A dependence on the target material was observed and an inverse proportionally of the number of projectiles needed to achieve charging up and the deposited

projectile energy in the electronic stopping regime. This latter finding shows that charging-up is related to secondary electron ejection. A most puzzling question remains, however, unanswered: Is the observed charging up a (macroscopic?) surface- or a (microscopic?) bulk phenomenon? Or, do both processes contribute? The finding that sandwich targets with gold layers on both surfaces behave in the same way as pure insulators, whereas a single gold layer screened the outgoing electron, points toward a possible bulk contribution.

ACKNOWLEDGMENTS

Special thanks to the LNS-CS staff for providing excellent ion beams. Thanks to N. Giudice, A. Grimaldi, N. Guardone, V. Sparti, and S. Urso from INFN Sez. Catania; V. Campagna, G. De Luca, A. Di Stefano, and A. Salomone from INFN-LNS for technical assistance and to C. Marchetta and E. Costa for target preparation. Three of us (S.H., H.R., and C.V.) thank their Sicilian colleagues for their great hospitality and INFN for financial support.

[1] H. Rothard and B. Gervais, Mat. Fys. Medd. Dan. Vidensk. Selsk. **52**, 497 (2006).
[2] L. K. Monteith and J. R. Hauser, J. Appl. Phys. **38**, 5355 (1973).
[3] B. Gross, J. Dow, and S. V. Nablo, J. Appl. Phys. **44**, 2459 (1973).
[4] J. Cazaux, Nucl. Instrum. Methods Phys. Res. Sect. B **244**, 307 (2006).
[5] J. A. Davies, W. N. Lennard, and I. V. Mitchell, in *Handbook of Modern Ion Beam Materials Analysis,* edited by J. R. Tesner, M. Nastasi, J. C. Barbour, C. J. Maggiore, and J. W. Mayer (Materials Research Society, Pittsburgh, 1995), Chap. 12.
[6] Y. Kanai, M. Hoshino, T. Kambara, T. Ikeda, R. Hellhammer, N. Stolterfoht, and Y. Yamazaki, Phys. Rev. A **79**, 012711 (2009).
[7] N. Stolterfoht, R. Hellhammer, Z. Juhász, B. Sulik, V. Bayer, C. Trautmann, E. Bodewits, A. J. de Nijs, H. M. Dang, and R. Hoekstra, Phys. Rev. A **79**, 042902 (2009).
[8] K. Schiessl, W. Palfinger, K. Tökési, H. Nowotny, C. Lemell, and J. Burgdörfer, Phys. Rev. A **72**, 062902 (2005).
[9] Y. Iwai, T. Ikeda, T. M. Kojima, Y. Yamazaki, K. Maeshima, N. Imamoto, T. Kobayashi, T. Nebiki, T. Narusawa, and G. P. Pokhil, Appl. Phys. Lett. **92**, 023509 (2008).
[10] G. Lanzanò *et al.*, Nucl. Phys. A **683**, 566 (2001).
[11] G. Lanzanó *et al.*, Phys. Rev. A **58**, 3634 (1998).
[12] G. Lanzanó *et al.*, Phys. Rev. Lett. **83**, 4518 (1999).
[13] G. Lanzanó *et al.*, Phys. Rev. A **63**, 032702 (2001).
[14] E. De Filippo *et al.*, Phys. Rev. A **68**, 024701 (2003).
[15] E. De Filippo, G. Lanzanó, H. Rothard, and C. Volant, Phys. Rev. Lett. **100**, 233202 (2008).
[16] G. Lanzanó, E. De Filippo, S. Hagmann, H. Rothard, and C. Volant, Radiat. Eff. Defects Solids **162**, 303 (2007).
[17] H. Rothard *et al.*, Phys. Rev. A **51**, 3066 (1995).
[18] M. Jung, H. Rothard, B. Gervais, J. P. Grandin, A. Clouvas, and R. Wünsch, Phys. Rev. A **54**, 4153 (1996).
[19] E. De Filippo, G. Lanzanó, S. Hagmann, and H. Rothard, LNS Activity Report 2007 (2008) 23. [http://www.lns.infn.it/index.php?option=com_docman&Itemid=164].
[20] H. Rothard, G. Lanzanó, D. H. Jakubassa-Amundsen, E. De Filippo, and D. Mahboub, J. Phys. B **34**, 3261 (2001).
[21] M. Burkhard, H. Rothard, C. Biedermann, J. Kemmler, P. Koschar, and K. O. Groeneveld, Nucl. Instrum. Methods B **24/25**, 143 (1987).
[22] G. Xiao, G. Schiwietz, P. L. Grande, N. Stolterfoht, A. Schmoldt, M. Grether, R. Köhrbrück, A. Spieler, and U. Stettner, Phys. Rev. Lett. **79**, 1821 (1997).
[23] G. Schiwietz, K. Czerski, M. Roth, F. Staufenbiel, and P. L. Grande, Nucl. Instrum. Methods B **226**, 683 (2004).
[24] J. F. Ziegler, J. P. Biersack, and U. Littmark, *The Stopping and Range of Ions in Solids* (Pergamon Press, New York, 1985, 2009).
[25] N. Bundaleski, H. Khemliche, P. Rousseau, A. Cassimi, L. Maunoury, and P. Roncin, J. Phys.: Conf. Series **163**, 012091 (2009).
[26] A. R. Blythe, *Electrical Properties of Polymers*, Cambridge Solid State Science Series (Cambridge University Press, Cambridge, 1980).